Research Article

One-step ball milling synthesis of VO_2 (M) nanoparticles with exemplary thermochromic performance

Chiyuan Wang[1] · Huiyan Xu[1] · Tongyao Liu[1] · Shuaijun Yang[1] · Yong Nie[1] · Cheng Wang[1] · Xiaodan Guo[1] · Binbin Wang[1] · Xin Ma[1] · Xuchuan Jiang[1]

Received: 17 November 2020 / Accepted: 4 January 2021 / Published online: 8 March 2021

Abstract
Vanadium dioxide (VO_2) has demonstrated highly potential for smart windows because of its thermochromic property. This study represents the development of a facile but efficient method for the synthesis of VO_2 (M) nanoparticles by ball milling method under ambient conditions, without release of waste liquid or gases. The key variables related to synthesis, including milling time and molar ratio of raw materials, have been investigated. It was found that the pure-phase VO_2 (M) nanoparticles with the sizes of the particles ranged from 20 to 50 nm and relatively good dispersivity could be prepared by optimizing process parameters. For practice use to decrease the phase transition temperature, elemental W doping amount of 2 at.%, $V_{1-x}W_xO_2$ (M) nanoparticles were also studied, and their glass coating exhibits high thermochromic performance with luminous transmittance (T_{lum}) of 44.18%, solar regulation efficiency (ΔT_{sol}) of 9.64%, and the critical phase transition temperature (T_c) of ~ 42 °C. This work demonstrates a green and promising ball milling method to fabricate large scale VO_2 (M) and $V_{1-x}W_xO_2$ (M) nanoparticles for smart windows.

Keywords Vanadium dioxide · Ball milling · Nanoparticles · Smart coatings

1 Introduction

Vanadium dioxide (VO_2) undergoes a reversible metal-to-insulator (MIT) transition at a critical temperature of 68 °C, accompanied with dramatic changes in optical and electrical properties [1]. Since the phase-transition property of VO_2 (M) was firstly reported by Morin in 1959, [2] it has been studied widely for application in thermochromic smart windows [3–5].

A variety of approaches have been explored to prepare VO_2 (M) particles or films. The main techniques employed to construct nanostructures of thermochromic VO_2 (M) are vapor deposition method, [6, 7] combustion method, [8] hydrothermal method, [9–11] sol–gel method, [12, 13] electrochemical method [14, 15] and solution methods [16, 17]. Among them, vapor deposition is an efficient method to fabricate high quality VO_2 (M)-film, but the equipment is usually complex and expensive. Combustion-assist fabrication is a cost effective and simple method to prepare VO_2 (M), but the violent reaction and uneven heat distribution during the combustion process result in the broad particle size distribution varying from 50 nm to 10 μm [18]. Fortunately, hydrothermal method can solve this problems mentioned above due to its controllability in particle size, morphology, and phase structure of VO_2 (M) nanoparticles. However, hydrothermal reaction is usually accompanied with high pressure (6.45–9.28 Mpa), [19] long reaction time (6–72 h) [9, 20, 21] and effluent disposal, which exists

Supplementary Information The online version contains supplementary material available at (https://doi.org/10.1007/s42452-021-04154-x).

✉ Huiyan Xu, ism_xuhy@ujn.edu.cn; ✉ Xuchuan Jiang, ism_jiangxc@ujn.edu.cn | [1]Institute for Smart Materials & Engineering, University of Jinan, Shandong 250022, China.

security risks and leads to the serious environmental pollution. Therefore, it is necessary to look for a novel method to synthesis the high quality VO_2 (M) nanoparticles with mild condition, simple process and environmental protection.

Recently, the facile ball milling method to synthesize VO_2 (M) has attracted much attention due to its own advantages, such as shorter preparation time, and less pollution than hydrothermal methods. Furthermore, this method has a good application prospect in large-scale production. Billik et al. [22] prepared the VO_2 (M) nanoparticles by ball milling V_2O_5 and Na_2SO_3. However, the washing procedure partially leads to the reaction of VO_2 (M) with water and produces some other phases. Chika Takai et al. [23] obtained the pure VO_2 (M) particles by controlling the addition of paraffin wax and milling time, but the particles agglomerated severely. To sum up, the ball milling method is a green technique to prepare VO_2 (M) on a large scale, but the preparation of the high quality VO_2 (M) nanoparticles by this method remains a challenge, which need to be further optimized.

Herein, the pure VO_2 (M) nanoparticles with particle size ranging from 20 to 50 nm (average size of ~ 42 nm) and relatively good dispersivity are obtained by a facile one-step ball milling method with carbon as the reductant. Specifically, the variables, such as reaction time and molar ratio of reaction materials have been studied systematically. Furthermore, the low-temperature (300 °C) treatment can improve the ΔT_{sol} of VO_2 (M) film from 6.38 to 9.12%, due to the enhanced crystallinity of VO_2 (M). Meanwhile, the W-doping can decrease the T_c of $V_{1-x}W_xO_2$ (M) greatly, and the excellent thermochromic performance with great ΔT_{sol} (9.64%), high T_{lum} (44.18%) and low T_c (42 °C) could be obtained while W doping content is 2 at.%, which has good potential for practical application in smart window.

2 Experimental section

2.1 Ball milling preparation of VO_2 (M)

VO_2 (M) nanoparticles were prepared by high energy mill (model 8000D Mixer) under air condition with milling rotational speed of 1425 rpm. The optimum value of the ball-to-powder weight ratio was 30:1.

The mole ratio of reaction and the milling time were investigated. Firstly, the mixture of different molar ratios (2:0.5–2:8) V_2O_5 (98%, Wuxi Zhan Wang chemical reagent, Ltd.): activated carbon (AR, Tianjin Da Mao chemical reagent, Ltd.) was milled for 1 h. Then, the raw materials were milled with the optimum molar ratio of 2:1 for different time (0 min, 10 min, 30 min, 1 h, 2 h, 4 h). Subsequently, the samples were separated from the milling vessel and washed 3 times by DI water and alcohol, then dried in an oven at 80 °C for 6 h.

We also prepared tungsten (W) doped VO_2 (M) by adding tungsten acid (99%, Shanghai Macklin Biochemical Co, Ltd.) (1%, 2% and 3% W/V molar ratio of W) and milled with V_2O_5: activated carbon of 2:1 for 2 h. After milling, the samples were separated from the milling vessel and washed 3 times by DI water and alcohol (AR, Sinopharm Chemical Reagent Co, Ltd.), and dried in an oven at 80 °C for 6 h. In the end, all of them were treated at 300 °C for 4 h in a vacuum atmosphere.

2.2 Synthesis of VO_2 (M) thermochromic films

Firstly, 0.05 g as-prepared VO_2 (M) powder was dispersed ultrasonically in 10 mL ethyl alcohol for 30 min. Then 0.6 g polyvinyl butyral (PVB, Shanghai Macklin Biochemical Co, Ltd.) was added into the VO_2 (M) dispersion with constant stirring at room temperature until complete dissolution. The mixture was uniformly cast onto the microscope slide substrate by 41 μm roller bar with the speed of 50 m/min for three times. Then, the films were dried at 80 °C for 6 h to remove the ethanol. Finally, thermochromic films were obtained.

2.3 Characterization

The crystal structures of the as-prepared samples were determined by X-ray diffraction (XRD, D8 Focus, Bruker AXS Gmbh, Germany) performed using a Cu–Kα radiation source (λ = 1.54056 Å), with a speed of 4°/min in a 2θ range from 10° to 80° at room temperature. The morphology of the nanoparticles and film were examined by scanning electron microscopy (SEM, MIRA3, TESCAN, Czech Republic) and transmission electron microscopy (TEM, JEM-2100F, JEOL, Tokyo, Japan). Thermal properties were detected by differential scanning calorimetry (Discovery DSC 2500, TA, New Castle, America) at a heating/cooling rate of 10 °C min^{-1} under nitrogen flow with temperature ranging from 0 to 100 °C.

Thermochromic switching parameters were monitored on an UV-vis-NIR spectrophotometer (SHIMADZU UV-3600 Plus) equipped with a temperature controlling unit.

The integrated luminous transmittance (T_{lum}, 380–780 nm) and solar transmittance (T_{sol}, 250–2500 nm) were essential, which could be obtained from the following equation.

$$T_{lum(sol)} = \int \varphi_{lum(sol)}(\lambda)T(\lambda)d\lambda / \int \varphi_{lum(sol)}(\lambda)d\lambda$$

where $T(\lambda)$ denotes the transmittance at wavelength λ, $\varphi_{lum}(\lambda)$ is the spectral sensitivity of the light-adapted eye, and $\varphi_{sol}(\lambda)$ is the solar irradiance spectrum for air mass 1.5

corresponding to the sun standing 37° above the horizon [24, 25]. As a result, the ΔT_{sol} could be calculated.

3 Results and discussion

3.1 One-step ball milling synthesis of VO_2 (M) nanoparticles

Figure 1a shows the XRD patterns of samples milled with different molar ratios of V_2O_5 to activated carbon (2:0.5–2:8) for 1 h. The small diffraction peaks of VO_2 (M) (JCPDS no. 043-1051) appear when the molar ratio is 2:0.5, which suggests that V_2O_5 can be effectively reduced to VO_2 by activated carbon during ball milling process. With further increase of the carbon content, all the diffraction peaks are corresponding to VO_2 (M) when the molar ratio is 2:1. However, the peak intensity decreases when further decreases the molar ratio, indicating that the excess carbon can reduce the crystallinity, which may be due to that the impurity atoms penetrate interstitial sites in the milling process [26].

In order to explore the formation of VO_2 (M) in the ball milling process, the mixture of V_2O_5 and C with the molar ratio of 2:1 has been milled for different time. As shown in Fig. 1b, the diffraction peaks of VO_2 (M) gradually generate with prolongation of the milling time to 1 h, and the diffraction peak intensity of VO_2 (M) significantly decreases with further increase of the milling time. This phenomenon indicates that the excessive milling process can reduce the crystallinity of VO_2 (M), which may be because of the accumulated lattice defects in VO_2 (M) [27].

The morphology and size of the mixture milled for different time could be observed from the SEM picture in Fig. 2. It reveals that the raw V_2O_5 contains large particles, and the particle size decreased sharply after milled for 10 min, as shown in Fig. 2b. With further increase of milling time, the particle size gradually decreased, and the smallest particle with size from 20 to 50 nm (average size of 42 nm) can be obtained when the milling time is 2 h. However, as shown in Fig. 2f, the particles aggregated severely when further increase the milling time to 4 h, which can severely degrade the thermochromic performance.

In order to confirm the reaction mechanism, the clear $Ca(OH)_2$ aqueous and the 0.1 wt.% $PdCl_2$ solution are used to detect the gaseous product obtained during ball milling process. The gas is collected by polythene plastic bag, and then inject into the airtight vial containing indicator. As can be seen in Fig. S1, the indicator of pellucid $Ca(OH)_2$ solution markedly become turbid after injecting the gas, while the indicator of $PdCl_2$ solution still remained clarification, demonstrating that the gaseous product is CO_2 rather than CO. Thus, the reaction in the milling process can be proposed as the following:

$$2V_2O_5 + C \rightarrow 4VO_2(M) + CO_2 \uparrow$$

As shown in Fig. 3, in the ball milling collision process, the particle size decreased rapidly, which can increase the surface energy of raw material. In addition, it is reported that the temperature of the particle surface (1 μm^2) can reach up to 1000 K with the duration of 10^{-4}–10^{-3} s in the collision process [28–30]. Benefited by the increased surface energy of raw materials and instantaneous high temperature during collision process, V_2O_5 has been reduced to VO_2 (M) by carbon.

The phase transition temperature of VO_2 (M) can be investigated by DSC analysis, due to its first-order reversible phase transition companied with energy absorbed and released during heating and cooling processes. Figure 4a shows the DSC curves of the VO_2 (M) obtained by ball milling for 2 h. A typical metal-insulator transition characteristic could be detected in the sample, which the DSC curves show endothermic peaks at about 72.1 °C during the heating process and exothermic peaks at about 55.4 °C during the cooling process. Besides that, vis-near-infrared transmittance spectra of the composite film of VO_2 (M) is characterized at 15 °C (before phase transition) and 100 °C (after phase transition) for detecting its optical modulation

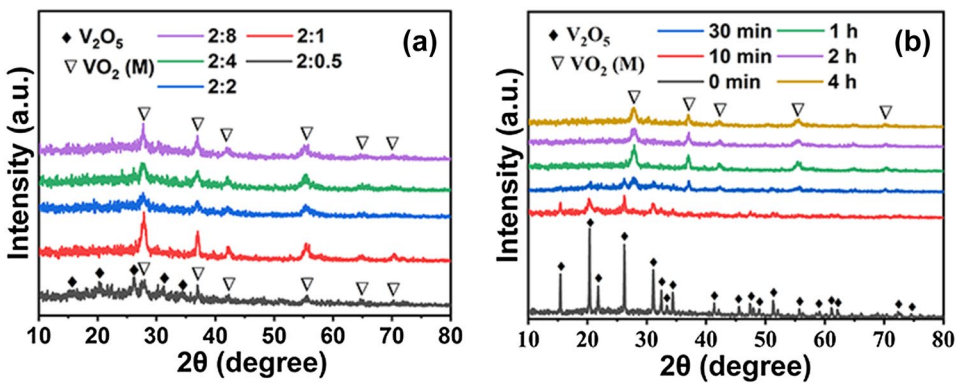

Fig. 1 XRD patterns of **a** the mixture of the V_2O_5 and activated carbon with different molar ratios of V_2O_5 to activated carbon milled for 1 h, **b** the mixture of V_2O_5 : C = 2:1 milled for different time

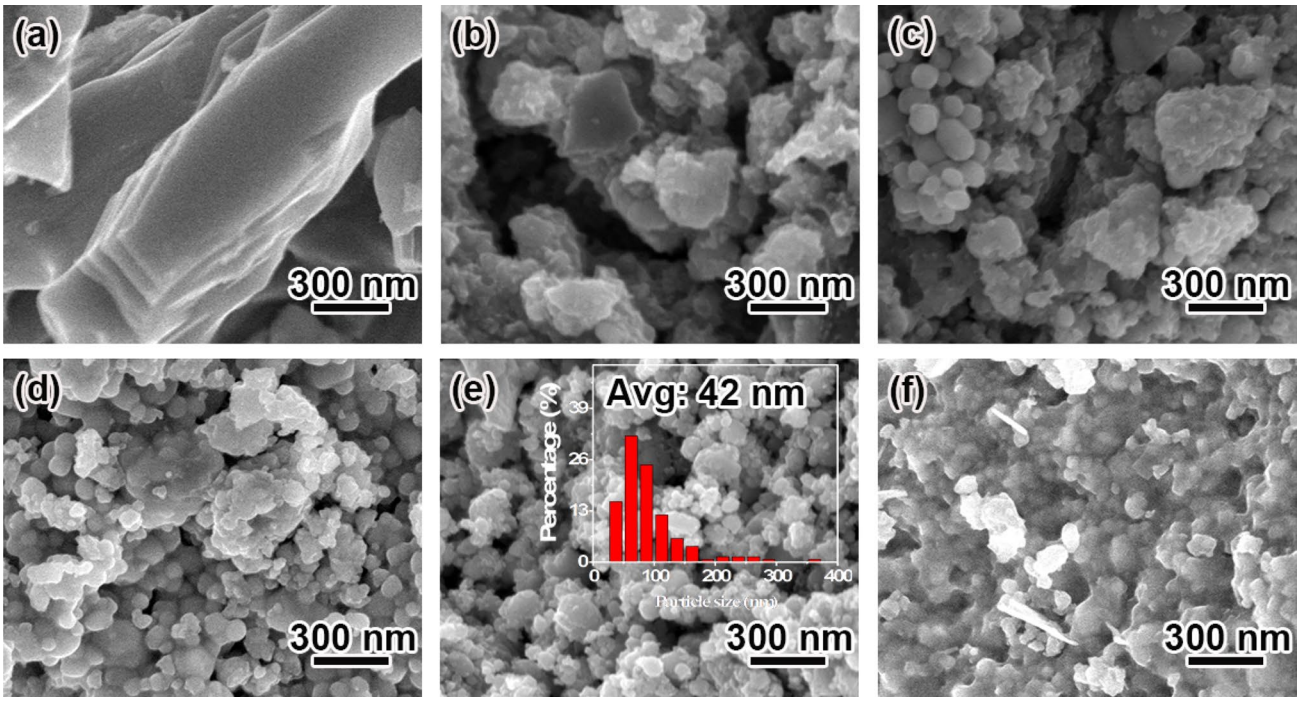

Fig. 2 SEM images of **a** the commercial V_2O_5 and mixture of V_2O_5 : C = 2:1 milled for **b** 10 min, **c** 30 min, **d** 1 h, **e** 2 h, **f** 4 h. (the insert is the particle size statistics from 150 NPs)

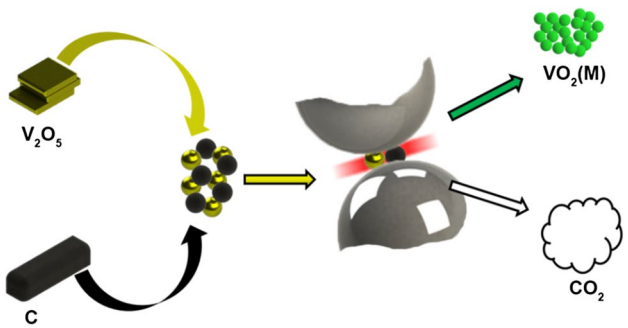

Fig. 3 Schematic illustration of possible reaction occurring in the milling process

capability, as shown in Fig. 4b. The transmittance spectrum of VO_2 (M) film exhibits high T_{lum} (380–780 nm) of 52.78% and great ΔT_{sol} (250–2500 nm) of 6.38% (Fig. 4b), indicating the VO_2 (M) nanoparticles prepared by ball milling method have great potential for practical application in smart windows.

3.2 Low-temperature treatment

The thermochromic performance is not only determined by particle size, but also by crystallinity [4]. In order to further improve the thermochromic performance of the VO_2 (M) nanoparticles synthesized by one-step ball milling,

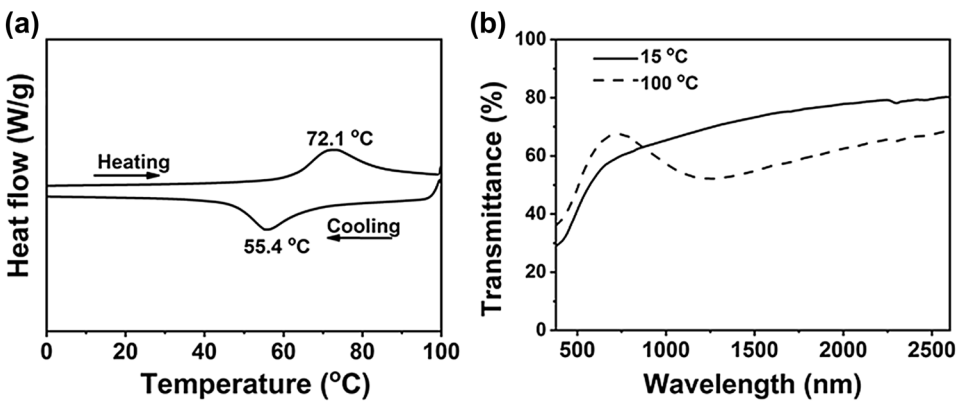

Fig. 4 **a** DSC curves of the VO_2 (M) obtained by ball milling for 2 h with V_2O_5 : C = 2:1, **b** Optical transmittance spectra at low and high temperature of the VO_2 (M)

the powder is treated at different temperature from 300 to 800 °C. As shown in Fig. 5a, the peak intensity is relatively stronger after low-temperature (300 °C for 4 h) treatment, indicating that the crystallinity of VO_2 (M) is obviously enhanced. Fortunately, the particle size remains unchanged after low-temperature treatment. However, the nanoparticles grow into elongated nanorods when the temperature is increased to 400–800 °C, as clearly shown in Figs. S2(b–d). Figure 5c and d show the TEM images of the original VO_2 (M) and the low-temperature treated VO_2 (M) particles. Figure 5e illustrates the HRTEM image of the nanoparticle circled in Fig. 5c. Compared with the original VO_2 (M) particles (Fig. 5c), the low-temperature treated VO_2 (M) particles exhibit much more clear lattice fringes, and the interplanar distance of d = 3.2 Å can still be indexed to the (011) planes of monoclinic VO_2 (Fig. 5f). Meanwhile, the distinct lattice fringes verify that the crystallinity of the low-temperature treated VO_2 (M) particles has been enhanced compared with the original VO_2 (M) particles, which is in consistence with XRD results. It indicates that the low temperature treatment is beneficial to maintain original morphology of VO_2 (M), as well as improve crystallinity of VO_2 (M) and further promote the thermochromic property.

In order to clarify the positive effect of low-temperature treatment on the thermochromic performance of VO_2 (M), the transmittance spectra of films based on original VO_2 (M) and low-temperature treated VO_2 (M) have been detected. As shown in Fig. 6, it can be seen that the thermochromic performance of the low-temperature treated VO_2 (M) film (T_{lum}, ~ 50.45%; ΔT_{sol}, ~ 9.12%) is improved when compared with the original VO_2 (M) film (T_{lum}, ~ 52.78%; ΔT_{sol}, ~ 6.38%). It indicates that the low-temperature treatment can obviously enhance the thermochromic performance of VO_2 (M).

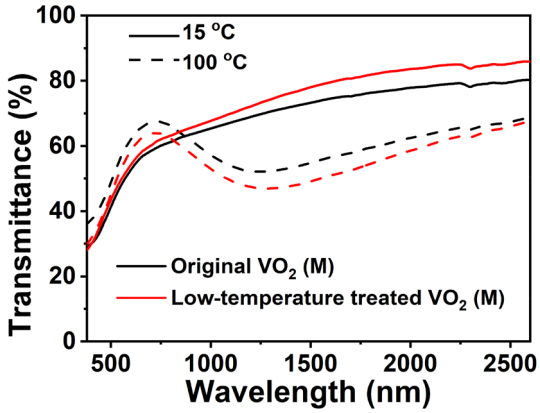

Fig. 6 Optical transmittance spectra at low and high temperature of the original VO_2 (M) and low-temperature treated VO_2 (M)

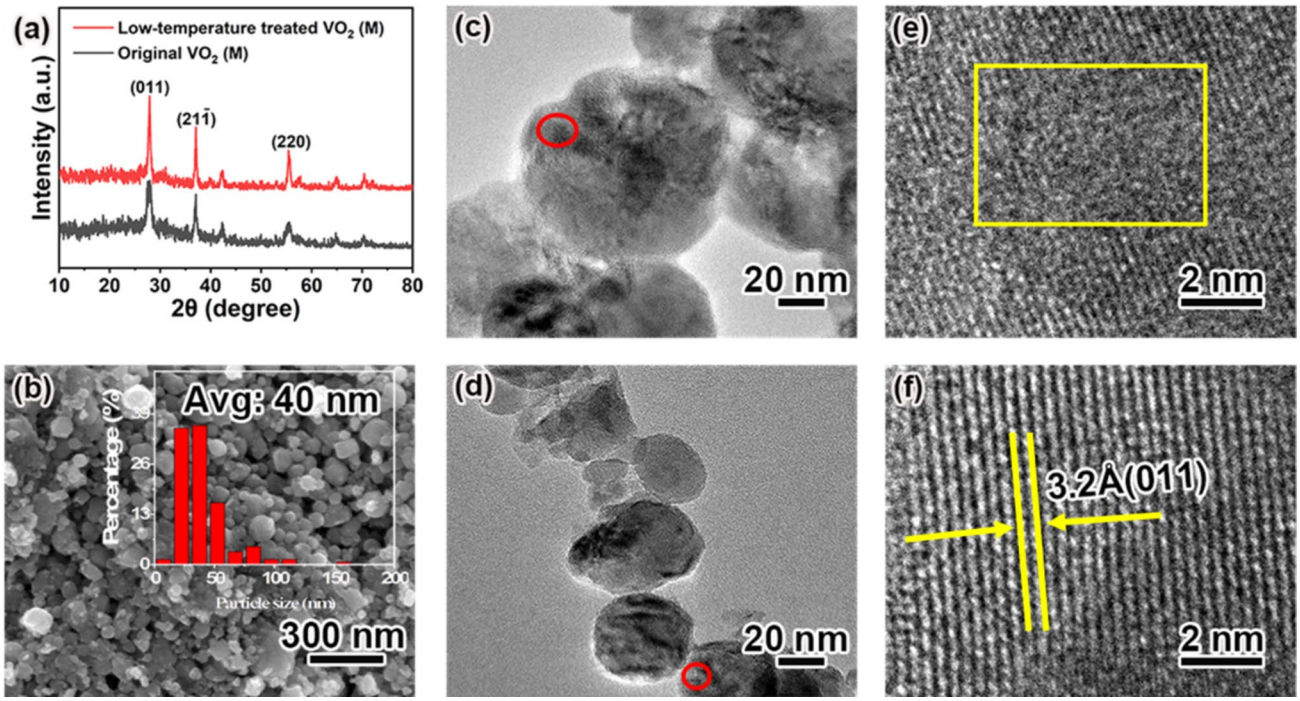

Fig. 5 **a** XRD patterns of the original VO_2 (M) obtained by ball milling with ball milling time of 2 h and molar ratio of V_2O_5 : C = 2:1, and the low-temperature treated VO_2 (M) at 300 °C, **b** SEM images of the low-temperature treated VO_2 (M), **c** and **d** TEM images of the original VO_2 (M) and the low-temperature treated VO_2 (M) particles, **e** and **f** HRTEM images of the nanoparticles circled in (**c**) and (**d**) respectively

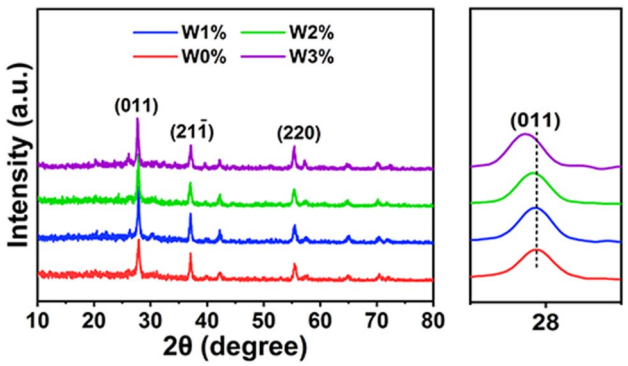

Fig. 7 XRD patterns of the $V_{1-x}W_xO_2$ (M). (0%, 1%, 2%, and 3% indicate the W/V molar ratio of W doped VO_2 (M))

Table 1 The d-spacing of (011) plane for VO_2 (M) with different W doping amounts

Sample	W-doped amount (at.%)	D-spacing (Å)
W0%	0	3.196
W1%	1	3.199
W2%	2	3.200
W3%	3	3.214

3.3 W-doped VO_2 (M) nanoparticles

In order to decrease the T_c of VO_2 (M), tungsten element as the dopant is used in our experiment. Figure 7 shows the XRD patterns of the low-temperature treated VO_2 (M) particles with different doping amounts of W element. Obviously, the diffraction peaks (011) are found to monotonously shift toward a smaller angle with the increase of the W doping amount, and the d-spacing of VO_2 (011) plane calculated by the Bragg's Law (Table 1) increases with the enhancement of the W-doping concentration. This phenomenon can be attributed that the W^{6+} ions with larger radius has successfully substituted V^{4+} ions, [31] indicating that the W element has been effectively doped in the VO_2 (M). The morphology of the $V_{1-x}W_xO_2$ (M) with various W-doped contents is characterized by SEM, as shown in Fig. S2. The morphology of the $V_{1-x}W_xO_2$ (M) nanoparticles basically remain and the average particle size is ~ 40 nm. It demonstrates that the W-doping has little influence on the morphology and the size of VO_2 (M).

As shown in Fig. 8a, the DSC curves of the $V_{1-x}W_xO_2$ (M) with various W-doped contents confirm the effect of W doping on the thermal properties of $V_{1-x}W_xO_2$ (M). As expected, the pure VO_2 (M) after low-temperature treatment exhibited a T_c value of 67.7 °C. For W-doped VO_2 (M), the T_c value of the W-doped VO_2 (M) reduced from 67.7 to 27.1 °C with W-doped concentration increased from 0 to 3 at.% W doping, respectively. And the T_c of the $V_{1-x}W_xO_2$ (M) decreases with a rate of 13.5 °C per at.% W, which agrees well with the reported results [25]. Further analysis of the DSC curves (Fig. 8b) reveals that thermal hysteresis width (ΔT_c) sharply decreases with increasing W doping amount, indicating that the phase transition of vanadium dioxide becomes more sensitive with the increase of doping amount.

Figure 8c exhibits the transmittance spectra of the films based on $V_{1-x}W_xO_2$ (M) with the uniform thickness (W0%, ~ 1.6 μm, W1%, ~ 1.7 μm, W2%, ~ 1.4 μm, W3%, ~ 1.5 μm, Fig. S4) and the calculated optical performance (ΔT_{sol} and T_{lum}) is summarized in Table 2. Clearly, as the W doping amount increases from 0 to 3 at.%, the T_{lum} and ΔT_{sol} of $V_{1-x}W_xO_2$ (M) decreases from 50.45% and 9.12% to 46.56% and 2.45%, respectively. This is due to the poor crystallinity and serious lattice distortion induced by additional point defects [11, 25, 32, 33].

Table 3 summarizes the thermochromic properties of VO_2 (M) films obtained by different methods in recent years. Compared to other methods, VO_2 (M) obtained by the hydrothermal methods exhibit better thermochromic properties. Guo et al. [34] reported that the undoped VO_2 (M) nanoparticles with average size of ~ 30 nm synthesized by hydrothermal method exhibit excellent thermochromic performance with the solar modulation efficiency of 12.34% and luminous transmittance of 54.26%. Dai et al. [11] reported F-doped VO_2 nanoparticles, which had lower phase transition temperature of 35 °C at 2.93 at.% F and

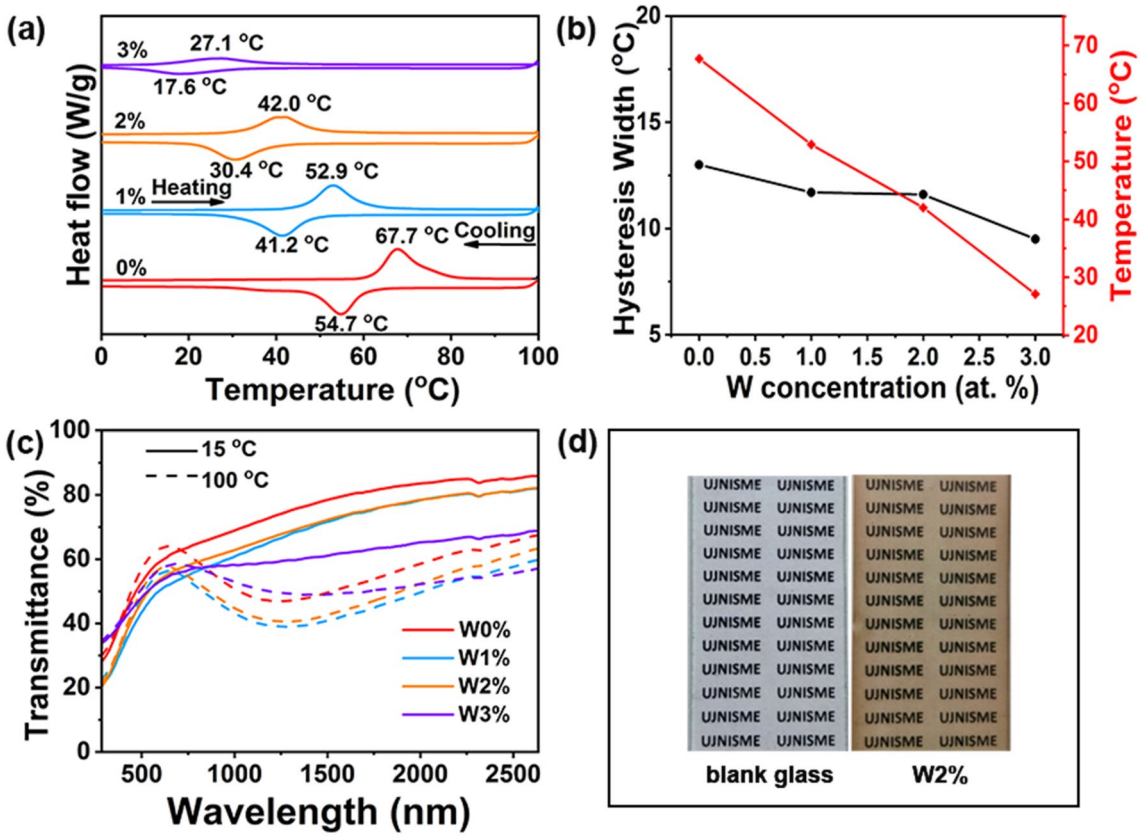

Fig. 8 **a** DSC curves of the $V_{1-x}W_xO_2$ (M), **b** the dependence of hysteresis width on the doping levels. **c** Optical transmittance spectra at low and high temperature of the $V_{1-x}W_xO_2$ (M), **d** Photograph of blank glass and complex film of the $V_{1-x}W_xO_2$ (M) with 2% W-doped content

Table 2 Summary of the optical properties for samples: original VO_2 (M) and $V_{1-x}W_xO_2$ (M) with different W-doped amounts

Sample	T_{lum}(%)		T_{sol} (%)		ΔT_{sol} (%)
	15 °C	100 °C	15 °C	100 °C	
Original VO_2 (M)	52.78	57.51	63.98	57.60	6.38
W0%	50.45	53.87	62.41	53.29	9.12
W1%	41.10	45.12	54.17	45.19	8.98
W2%	44.18	47.19	56.33	46.69	9.64
W3%	46.56	48.92	54.01	51.56	2.45

exhibited great optical performance with ΔT_{sol} of 10.7% and T_{lum} of 48.7%, which is similar with our 2 at.% W doped VO_2 with ΔT_{sol} of 9.64%, T_{lum} of 44.18% and the T_c of around 42 °C.

Table 3 Summary of approaches to fabricate VO_2 (M) films

Method		Precursor	Condition	T_c	T_{lum} and ΔT_{sol}	References
Hydrothermal methods		$VOSO_4$ $N_2H_4{\cdot}H_2O$ NaOH	Hydrothermal reaction at 260 °C for 24 h	63 °C	T_{lum} = 54.26, ΔT_{sol} = 12.34%	[20]
		V_2O_5 $H_2C_2O_4{\cdot}2H_2O$ NH_4F	Hydrothermal reaction at 200 °C for 12 h, annealing under argon at 700 °C for 8 h	35 °C	T_{lum} = 48.7%, ΔT_{sol} = 10.7%	[11]
Vapor transport deposition methods	CVD	$VO(acac)_2$	The reaction at 440 °C, annealing under N_2 at 500 °C for 1 h	47 °C	T_{lum} = 61.6%, ΔT_{sol} = 6%	[6]
	PLD	TiO_2 ceramic / pure vanadium	The reaction at 400 °C	64 °C	T_{lum} = 53%, ΔT_{sol}= 5.2%	[35]
Combustion methods		NH_4VO_3 NH_4NO_3 $C_2H_5NO_2$	Flame	66 °C	N/A	[8]
This work		V_2O_5 C	Ball milling at room temperature for 2 h, low-temperature treatment at 300 for 4 h	42 °C	T_{lum} = 44.18%, ΔT_{sol} = 9.64%	

However, for the hydrothermal method, the high pressure is a potential security liability, the high reaction temperature (240 °C) and long reaction time (24 h) result in high cost and inefficiency, which hinder its industrialization. Compared to the hydrothermal method, ball milling method to prepare $V_{1-x}W_xO_2$ in our work is low-cost and high efficiency, which is suitable for mass production.

4 Conclusion

In this study, VO_2 (M) nanoparticles with particle size ranging from 20 to 50 nm (average size of ~ 42 nm) and relatively good dispersivity have been successfully synthesized by a facile ball milling method. The ball milling parameters are systematically studied and the optimum parameters are obtained. After low-temperature treatment, the ΔT_{sol} is improved from 6.38 to 9.12% due to the enhanced crystallinity of VO_2 (M). When W doping content is 2 at.%, the thermochromic film based on $V_{1-x}W_xO_2$ (M) nanoparticles can exhibit balanced ΔT_{sol} of 9.64%, T_{lum} of 44.18%, critical phase transition temperature of around 42.0 °C. This work may provide a simple, efficient, economic and environment-friendly approach for practical application in smart window.

Funding This work is supported by University of Jinan (XKY2069) and Shandong Shenna Smart Advanced Materials Co., Ltd.

Compliance with ethical standards

Conflict of interest The authors declare that they have no conflict of interest.

References

1. Budai JD, Hong J, Manley ME, Specht ED, Li CW, Tischler JZ, Abernathy DL, Said AH, Leu BM, Boatner LA, McQueeney RJ, Delaire O (2014) Metallization of vanadium dioxide driven by large phonon entropy. Nature 515(7528):535–539. https://doi.org/10.1038/nature13865
2. Morin FJ (1959) Oxides which show a metal-to-insulator transition at the neel temperature. Phys Rev Lett 3(1):34–36. https://doi.org/10.1103/PhysRevLett.3.34
3. Shi R, Shen N, Wang J, Wang W, Amini A, Wang N, Cheng C (2019) Recent advances in fabrication strategies, phase transition modulation, and advanced applications of vanadium dioxide. Appl Phys Rev 6(1):011312. https://doi.org/10.1063/1.5087864
4. Li M, Magdassi S, Gao Y, Long YJS (2017) Hydrothermal synthesis of VO_2 polymorphs: advantages, challenges and prospects for the application of energy efficient smart windows. Small 13(36):1701147. https://doi.org/10.1002/smll.201701147

5. Xu F, Cao X, Luo H, Jin P (2018) Recent advances in VO_2-based thermochromic composites for smart windows. J Mater Chem C 6(8):1903–1919. https://doi.org/10.1039/c7tc05768g
6. Top I, Binions R, Sol C, Papakonstantinou I, Holdynski M, Gaiaschi S, Abrahams I (2018) Improved thermochromic properties in bilayer films of VO_2 with ZnO, SnO_2 and WO_3 coatings for energy efficient glazing. J Mater Chem C 6(46):12555–12565. https://doi.org/10.1039/c8tc04543g
7. Warwick MEA, Roberts AJ, Slade RCT, Binions R (2014) Electric field assisted chemical vapour deposition – a new method for the preparation of highly porous supercapacitor electrodes. J Mater Chem A 2(17):6115–6120. https://doi.org/10.1039/c3ta14185c
8. Wu H, Qin M, Cao Z, Li X, Jia B, Chen P, Huang M, Qu X (2018) Direct synthesis of vanadium oxide nanopowders by the combustion approach. Chem Phys Lett 706:7–13. https://doi.org/10.1016/j.cplett.2018.05.064
9. Chen R, Miao L, Cheng H, Nishibori E, Liu C, Asaka T, Iwamoto Y, Takata M, Tanemura S (2015) One-step hydrothermal synthesis of $V_{1-x}W_xO_2$ (M/R) nanorods with superior doping efficiency and thermochromic properties. J Mater Chem A 3(7):3726–3738. https://doi.org/10.1039/c4ta05559d
10. Li W, Ji S, Sun G, Ma Y, Guo H, Jin P (2016) Novel VO_2 (M)–ZnO heterostructured dandelions with combined thermochromic and photocatalytic properties for application in smart coatings. New J Chem 40(3):2592–2600. https://doi.org/10.1039/c5nj02875b
11. Dai L, Chen S, Liu J, Gao Y, Zhou J, Chen Z, Cao C, Luo H, Kanehira M (2013) F-doped VO_2 nanoparticles for thermochromic energy-saving foils with modified color and enhanced solar-heat shielding ability. Phys Chem Chem Phys 15(28):11723–11729. https://doi.org/10.1039/c3cp51359a
12. Cao X, Wang N, Law JY, Loo SC, Magdassi S, Long Y (2014) Nanoporous thermochromic VO_2 (M) thin films: controlled porosity, largely enhanced luminous transmittance and solar modulating ability. Langmuir 30(6):1710–1715. https://doi.org/10.1021/la404666n
13. Kang L, Gao Y, Luo H, Chen Z, Du J, Zhang Z (2011) Nanoporous thermochromic VO_2 films with low optical constants, enhanced luminous transmittance and thermochromic properties. ACS Appl Mater Interfaces 3(2):135–138. https://doi.org/10.1021/am1011172
14. Minch R, Es-Souni M (2013) Nanostructured VO_2 thin films via cathodic deposition. CrystEngComm 15(34):6645. https://doi.org/10.1039/c3ce40848e
15. Cezar AB, Graff IL, Rikers Y, Schreiner WH, Mattoso N (2011) Highly oriented VO[sub 2] thin films prepared by electrodeposition. Electrochem Solid-State Lett 14(3):D23–D25. https://doi.org/10.1149/1.3525275
16. Cao X, Thet MN, Zhang Y, Joachim Loo SC, Magdassi S, Yan Q, Long Y (2015) Solution-based fabrication of VO_2 (M) nanoparticles via lyophilisation. RSC Adv 5(33):25669–25675. https://doi.org/10.1039/c4ra16840b
17. Lu Z, Li C, Yin Y (2011) Synthesis and thermochromic properties of vanadium dioxide colloidal particles. J Mater Chem 21(38):14776. https://doi.org/10.1039/c1jm12430g
18. Cao Z, Xiao X, Lu X, Zhan Y, Cheng H, Xu G (2016) A simple and low-cost combustion method to prepare monoclinic VO_2 with superior thermochromic properties. Sci Rep 6:39154. https://doi.org/10.1038/srep39154
19. Ji S, Zhang F, Jin P (2011) Selective formation of VO_2 (A) or VO_2 (R) polymorph by controlling the hydrothermal pressure. J Solid State Chem 184(8):2285–2292. https://doi.org/10.1016/j.jssc.2011.06.029
20. Guo D, Ling C, Wang C, Wang D, Li J, Zhao Z, Wang Z, Zhao Y, Zhang J, Jin H (2018) Hydrothermal one-step synthesis of highly dispersed M-phase VO_2 nanocrystals and application to flexible thermochromic film. ACS Appl Mater Interfaces 10(34):28627–28634. https://doi.org/10.1021/acsami.8b08908
21. Li W, Ji S, Li Y, Huang A, Luo H, Jin P (2014) Synthesis of VO_2 nanoparticles by a hydrothermal-assisted homogeneous precipitation approach for thermochromic applications. RSC Adv 4(25):13026–13033. https://doi.org/10.1039/c3ra47666a
22. Billik P, Čaplovičová M, Maňka J, Čaplovič Ľ, Cigáň A, Koňakovský A, Bystrický R, Dvurečenskij AJMSR (2011) Synthesis and transport properties of nanostructured VO_2 by mechanochemical processing. Meas Sci Rev 11(1):29–33. https://doi.org/10.2478/v10048-011-0001-6
23. Takai C, Senna M, Hoshino S, Razavi-Khosroshahi H, Fuji M (2018) Chemical and thermal properties of VO2 mechanochemically derived from V_2O_5 by co-milling with paraffin wax. RSC Adv 8(38):21306–21315. https://doi.org/10.1039/c8ra02159g
24. Chen Y, Zhu J, Ma H, Chen L, Li R, Jin P (2019) VO_2/Nickel-bromine-ionic liquid composite film for thermochromic application. Solar Energy Mater Solar Cells 196:124–130. https://doi.org/10.1016/j.solmat.2019.03.047
25. Zhu J, Zhou Y, Wang B, Zheng J, Ji S, Yao H, Luo H, Jin P (2015) Vanadium dioxide nanoparticle-based thermochromic smart coating: high luminous transmittance, excellent solar regulation efficiency, and near room temperature phase transition. ACS Appl Mater Interfaces 7(50):27796–27803. https://doi.org/10.1021/acsami.5b09011
26. Chakk Y, Berger S, Weiss B-Z, Brook-Levinson E (1994) Solid state amorphization by mechanical alloying—An atomistic model. Acta Metall et Mater 42(11):3679–3685. https://doi.org/10.1016/0956-7151(94)90433-2
27. Balaz P, Achimovicova M, Balaz M, Billik P, Cherkezova-Zheleva Z, Criado JM, Delogu F, Dutkova E, Gaffet E, Gotor FJ, Kumar R, Mitov I, Rojac T, Senna M, Streletskii A, Wieczorek-Ciurowa K (2013) Hallmarks of mechanochemistry: from nanoparticles to technology. Chem Soc Rev 42(18):7571–7637. https://doi.org/10.1039/c3cs35468g
28. Bowden FP, Yoff DA (1952) Initiation and growth of explosion in liquids and solids. J Chem Educ 1:326. https://doi.org/10.1119/1.1933188
29. Baláž P, Achimovičová M, Baláž M, Billik P, Cherkezova-Zheleva Z, Criado JM, Delogu F, Dutková E, Gaffet E, Gotor FJ, Kumar R, Mitov I, Rojac T, Senna M, Streletskii A, Wieczorek-Ciurowa K (2013) Hallmarks of mechanochemistry: from nanoparticles to technology. Chem Soc Rev 42(18):7571. https://doi.org/10.1039/c3cs35468g
30. James SL, Adams CJ, Bolm C, Braga D, Collier P, Friscic T, Grepioni F, Harris KD, Hyett G, Jones W, Krebs A, Mack J, Maini L, Orpen AG, Parkin IP, Shearouse WC, Steed JW, Waddell DC (2012) Mechanochemistry: opportunities for new and cleaner synthesis. Chem Soc Rev 41(1):413–447. https://doi.org/10.1039/c1cs15171a
31. Dong B, Shen N, Cao C, Chen Z, Luo H, Gao Y (2016) Phase and morphology evolution of VO_2 nanoparticles using a novel hydrothermal system for thermochromic applications: the growth mechanism and effect of ammonium (NH^{4+}). RSC Adv 6(85):81559–81568. https://doi.org/10.1039/c6ra14569h
32. Ji S, Zhang F, Jin P (2011) Preparation of high performance pure single phase VO_2 nanopowder by hydrothermally reducing the V_2O_5 gel. Solar Energy Mater Solar Cells 95(12):3520–3526. https://doi.org/10.1016/j.solmat.2011.08.015
33. Jin P, Nakao S, Tanemura SJTSF (1998) Tungsten doping into vanadium dioxide thermochromic films by high-energy ion implantation and thermal annealing. Thin Solid Films 324(1–2):151–158. https://doi.org/10.1016/S0040-6090(98)00362-9
34. Guo D, Ling C, Wang C, Wang D, Li J, Zhao Z, Wang Z, Zhao Y, Zhang J, Jin H (2018) Hydrothermal one-step synthesis of highly

dispersed M-phase VO_2 nanocrystals and application to flexible thermochromic film. ACS Appl Mater Interfaces 10(34):28627–28634. https://doi.org/10.1021/acsami.8b08908

35. Kang C, Zhang C, Zhang L, Liang S, Geng C, Cao G, Zong H, Li M (2019) Transformation of crystalline structure and photoelectric properties in VO_2/glass thin films by inserting TiO_2 buffer layers. Appl Surf Sci 463:704–712. https://doi.org/10.1016/j.apsusc.2018.08.193